

# ViSaRL: Visual Reinforcement Learning Guided by Human Saliency

Anthony Liang<sup>†</sup>, Jesse Thomason<sup>†</sup> and Erdem Bıyık<sup>†</sup>

**Abstract**— Training robots to perform complex control tasks from high-dimensional pixel input using reinforcement learning (RL) is sample-inefficient, because image observations are comprised primarily of task-irrelevant information. By contrast, humans are able to visually attend to task-relevant objects and areas. Based on this insight, we introduce Visual Saliency-Guided Reinforcement Learning (ViSaRL). Using ViSaRL to learn visual representations significantly improves the success rate, sample efficiency, and generalization of an RL agent on diverse tasks including DeepMind Control benchmark, robot manipulation in simulation and on a real robot. We present approaches for incorporating saliency into both CNN and Transformer-based encoders. We show that visual representations learned using ViSaRL are robust to various sources of visual perturbations including perceptual noise and scene variations. ViSaRL nearly doubles success rate on the real-robot tasks compared to the baseline which does not use saliency.

## I. INTRODUCTION

Studies in neuroscience [1] show that humans utilize selective attention to focus on task-relevant information for efficiently processing and understanding complex visual scenes [2]. We employ selective attention when performing everyday pick-and-place tasks to identify the target objects, focus on the grasp points, and execute precise hand-eye coordination. We hypothesize that saliency maps capturing human visual attention is a useful signal to process visual observations for AI agents. In this paper, we investigate whether *human* visual attention helps *agents* perform tasks.

A key ingredient in solving visual control tasks is to learn visual representations that capture useful features of the sensory input to simplify the decision making process. Many works in the deep reinforcement learning (RL) community have proposed to learn such representations through various self-supervised objectives including contrastive learning [3] and data augmentation [4]. By contrast, we focus on self-supervision using *saliency* as additional human domain knowledge to inform the representation of task-relevant features in the visual input while filtering out perceptual noise.

We present **Visual Saliency Reinforcement Learning** (ViSaRL), a general approach for incorporating human-annotated saliency maps as an inductive bias for learned visual representations. The key idea of ViSaRL is to train a visual encoder using both RGB and saliency inputs and an RL policy that operates over lower dimensional image representations as shown in Figure 1. By using a multimodal autoencoder trained using a self-supervised objective, our learned representations attend to the most salient parts of

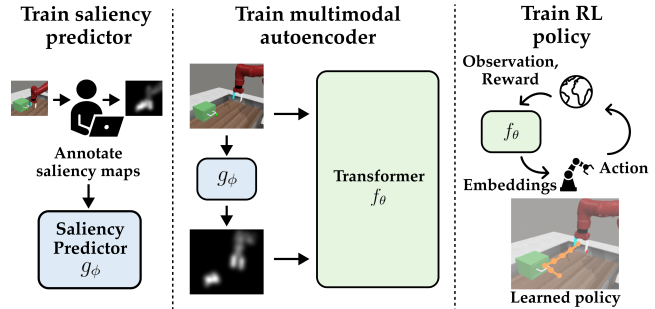


Fig. 1. ViSaRL trains a saliency prediction model from a few human-annotated saliency maps. This model is used to augment an offline image dataset with saliency. A visual encoder is pretrained with the paired image and saliency dataset and used during downstream policy learning to generate latent representations of the agent’s observations.

an image for downstream task learning making them robust to visual distractors. To circumvent the expensive process of manually annotating saliency maps, we train a state-of-the-art saliency predictor using only a few human-annotated examples to pseudo-label RGB observations with saliency.

We evaluate ViSaRL on a diverse set of challenging continuous control tasks in the DeepMind Control (DMC) suite [5] and robot manipulation tasks in Meta-World [6] and a real robot. Our method improves in sample-efficiency and robustness over state-of-the-art vision-based RL methods across all environments. Remarkably, ViSaRL nearly doubles the task success rate on a real-robot.

Our contributions can be summarized as follows: noitem-sep, nosep

- 1) We propose ViSaRL, a framework for incorporating human-annotated saliency maps to learn robust representations for visual control tasks;
- 2) We present approaches for utilizing saliency information in both CNN and Transformer encoders; and
- 3) We conduct extensive experiments that demonstrate ViSaRL consistently outperform prior state-of-the-art methods for various visual control tasks both in simulation and on a real robot.

## II. RELATED WORK

Different forms of human data can be leveraged when solving control tasks. Researchers have created various interfaces to collect different data modalities from humans such as reward sketches [7], feature traces [8], scaled comparisons [9], and abstract trajectories [10]. Attention saliency maps, in contrast, do not require humans to work with abstract concepts like rewards and task features, and do not require watching and comparing lengthy trajectories.

<sup>†</sup> Anthony Liang, Jesse Thomason, and Erdem Bıyık are with the Thomas Lord Department of Computer Science, University of Southern California, Los Angeles, CA 90089 USA. (Correspondence to: anthony.liang@usc.edu).

**Saliency Maps.** Saliency maps approximate which parts of an image tend to attract human visual attention, corresponding to where the human eye would likely fixate when viewing an image [11]. Saliency maps have been used in both computer vision and machine learning for various applications including activity recognition [12], question answering [13], and object segmentation [14]. The explainable AI community uses saliency maps to understand how a model is making its predictions and to identify the most informative regions of an image for a particular task [15], [16], [17]. Most existing works explore using saliency maps only as tools for interpretation [18], [19]. For example, Atrey et al. [18] and Rosynski et al. [19] use saliency maps to rationalize and explain the actions of RL agents in Atari games. Boyd et al. [20] show saliency maps encoding prior human knowledge enable better generalization of deep learning models.

Bertoin et al. [21] uses neural network saliency in a self-supervised regularization objective to encourage better visual representations. We do not use a model’s saliency, but rather human saliency to identify salient regions of the input image and distill this knowledge into the visual representation.

**User Interfaces for Human Saliency.** ViSaRL needs a small number of human-annotated saliency maps to bootstrap the saliency prediction network (Figure 1). Prior work used superpixel segmentation [22] to first divide each image into segments, and then asked humans to click on the segments that are salient [17]. However, that method requires manually checking and combining the segments that belong to the same object before showing the images to annotators, burdening system designers. As an alternative, Boyd et al. [23], [20] used interfaces where the annotators created binary masks by simply clicking on images. We employ a similar but simpler interface: an annotator clicks on the salient parts of the image, and a Gaussian kernel is applied around selected pixels to achieve smooth saliency maps.

**Representation Learning for RL.** Saliency maps are essentially representations of the environment that carry domain knowledge about which regions of the visual input are important for the downstream task. Such representations are crucial in RL because they enable agents to tractably deal with high-dimensional image observation spaces.

Prior works have shown that self-supervised learning with data augmentation helps achieve good performance in image-based RL. Contrastive Unsupervised RL (CURL) [3] employs a contrastive learning objective as an auxiliary loss to learn representations for off-policy RL. RL with Augmented Data (RAD) [24] and Data Regularized Q-Learning (DrQ) [4] use simple image augmentations such as random cropping and color jittering to provide strong regularization for learning representations invariant to visual perturbations. ViSaRL does not use data augmentation directly in the value function or policy update. Instead, saliency augmentation is introduced during the visual encoder pretraining phase.

Nair et al. [25] and Karamcheti et al. [26] propose to combine internet scale language and vision datasets with different self-supervised objectives to learn visual representations generally applicable across all robot tasks. While they

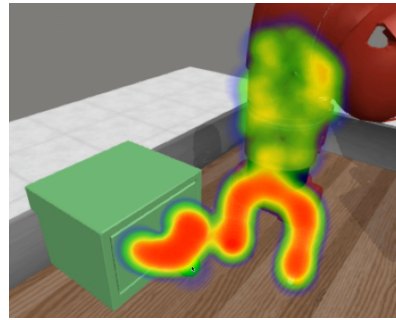


Fig. 2. **Annotation Interface.** Custom click-based saliency annotation interface. Each click generates a Gaussian centered at the clicked coordinate with some variance. Warmer colors denote more salient regions such as the drawer handle and the robot’s end-effector.

focus on learning general visual representations, ViSaRL augments small task-specific datasets with saliency information to improve pretrained visual representations.

Sax et al. [27] demonstrated that mid-level visual representations such as surface normals or depth predictions from RGB images removes unimportant information and captures useful invariances about the visual world leading to better success on downstream RL tasks. Similar to Sax et al. [27], ViSaRL utilizes saliency maps as a mid-level feature. However, we empirically show that our approach for incorporating the saliency information into the visual representation improves task performance over other mid-level features including depth and surface normals.

### III. VISUAL SALIENCY-GUIDED REINFORCEMENT LEARNING

We propose ViSaRL, a simple approach for incorporating human-annotated saliency to learn representations for visual control tasks. ViSaRL can be implemented on top of any standard RL algorithm for learning a policy. It aims to learn representations that encode useful task-specific inductive biases from human saliency maps. ViSaRL consists of three learned components: a saliency predictor  $g_\phi$ , an image encoder  $f_\theta$ , and a policy network  $\pi_\psi$ . Figure 1 provides an overview of the ViSaRL architecture. We will elaborate on each component in the following subsections.

**Saliency Predictor.** Saliency maps highlight regions in an image likely to capture human attention or are considered crucial for a given task. Having a human expert annotate saliency maps for every image observation is impractical and not scalable to complex domains. To alleviate the burden of manual annotations, we propose to learn a saliency network using only a few hand-annotated examples of saliency maps collected using a custom user interface.

Formally, given an input RGB image observation,  $I \in \mathbb{R}^{H \times W \times C}$ , a saliency predictor  $g_\phi$  maps an input image  $I$  to a continuous saliency map  $M = g_\phi(I) \in [0, 1]^{H \times W}$  highlighting important parts of the image for the downstream task. We use a state-of-the-art saliency model, Pixel-wise Contextual Attention network (PiCANet) [29]. PiCANet uses global and local pixel-wise attention modules to selectively

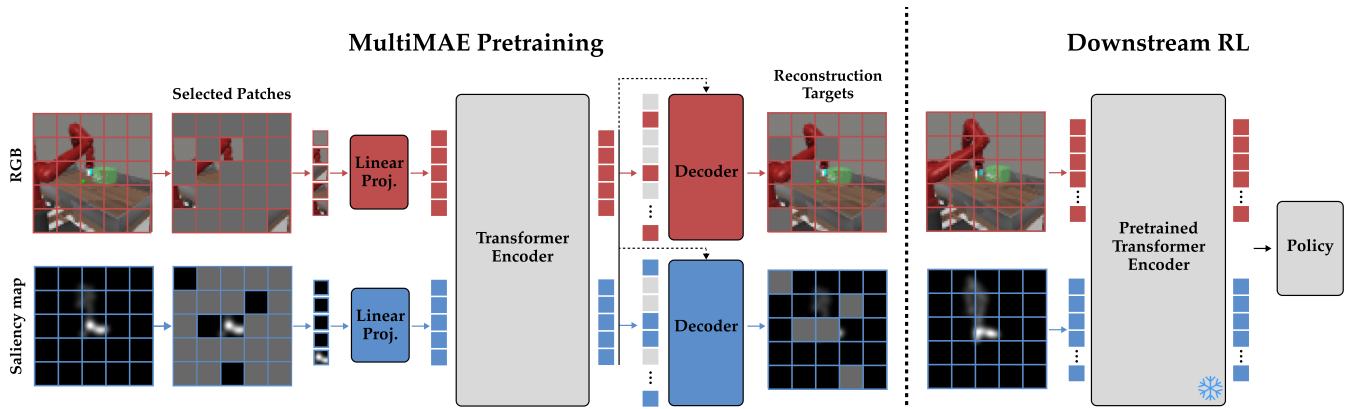


Fig. 3. **ViSaRL Approach.** We pretrain a MultiMAE [28] Transformer model on a dataset of paired RGB images and their saliency maps. MultiMAE employs a self-supervised training objective in which masked patches for both input modalities are reconstructed given only the visible patches. The pretrained model is frozen and used for extracting latent image representations during task learning. There is no input masking during downstream RL.

attend to informative context. Global attention can attend to backgrounds for foreground objects while local attention can attend to regions that have similar appearance. The mixture of attention at different scales allows for more homogeneous and consistent saliency predictions. We emphasize that our method is agnostic to the choice of saliency model.

**Pretraining Visual Representation.** We use our trained  $g_\phi$  to pseudo-label an offline image dataset collected using any behavior-policy (random, replay buffer, expert demonstrations, etc.) with saliency information. We then use the paired image and saliency dataset to pretrain an image encoder,  $f_\theta$ , for computing image embeddings. We experiment with two models for our backbone visual encoder, CNN and Transformer encoder, and investigate different techniques for augmenting each with saliency input. To add saliency to a CNN architecture, we can use saliency as a soft continuous mask or simply add saliency as an additional channel per pixel. For a Transformer encoder, we propose to pretrain the model with saliency as an additional input using a masked reconstruction objective.

Masked autoencoders (MAE) [30] are an effective and scalable approach for learning visual representations. MAE masks out random patches of an image and reconstructs the masked patches using a Vision Transformer (ViT) [31]. An image  $I \in \mathbb{R}^{H \times W \times C}$  is processed into a sequence of 2D patches  $h \in \mathbb{R}^{K \times (P^2 C)}$  where  $P$  is the patch size and  $K = HW/P^2$  is the number of patches. A subset of these patches are randomly masked out with a masking ratio of  $m$ . Only the *visible, unmasked patches* are used as input to the ViT encoder. Masking reduces the input sequence length and encourages learning global, contextualized representations from limited visible patches.

The image patches are first embedded via a linear projection and added to positional embeddings. The resulting tokens are processed via a series of Transformer blocks. Finally, a ViT decoder reconstructs the original input by processing all of the tokens including the encoded visible patches and placeholder mask tokens. Following He et al. [30], we employ a high masking ratio  $m = 0.75$

and a heavy-encoder, light-decoder architecture to enable efficiently learning good representations.

---

#### Algorithm 1 Visual Saliency-Guided RL

---

- 1: **Input:**  $\text{env}, \phi, \psi, \theta$  randomly initialized parameters
  - 2: Collect image dataset  $\mathcal{D}$  with any behavioral policy  $\pi_B$
  - 3: Annotate  $N$  random frames from  $\mathcal{D}$  with saliency
  - 4: Train  $g_\phi$  on  $\{(I, M)\}_{i=1}^N$  using PiCANet loss
  - 5: Annotate the full dataset  $\mathcal{D} = \{(I, g_\phi(I))\}_{i=1}^N$
  - 6: Train  $f_\theta$  using masked reconstruction
  - 7: **for** every environment step **do** ▷ RL Training
  - 8:     Select action  $a = \pi_\psi(f_\theta(o, g_\phi(o)))$
  - 9:     Optimize  $\mathcal{L}_{RL}$  wrt to  $\psi$
  - 10: **end for**
- 

**MultiMAE for Encoding Saliency.** The standard MAE architecture is limited to processing just RGB modality. We propose to incorporate saliency using the MultiMAE [28] architecture shown in Figure 3. MultiMAE extends MAE to encode multiple input modalities in a way that these modalities are contributing synergistically to the resulting representation. Specifically, MultiMAE uses a different linear projection and decoder for each input modality. A cross attention layer is used in each decoder to incorporate information from the encoded tokens of other modalities. Crucially, MultiMAE’s pretraining objective requires the model to perform well in both the original MAE objective of RGB in-painting and cross-modal reconstruction, resulting in a stronger cross-modal visual representation.

**Downstream Policy Learning.** After pretraining the MultiMAE model, we freeze the encoder and use it to compute latent representations of environment observations for policy training. ViSaRL is not only compatible with online RL algorithms such as Soft-Actor Critic (SAC) [32] in which the agent learns through environment interactions but also imitation learning from expert demonstrations. Image inputs are not masked during policy learning. We average the patch embeddings to generate a global image representation. We also tried using the global learned token embedding, similar

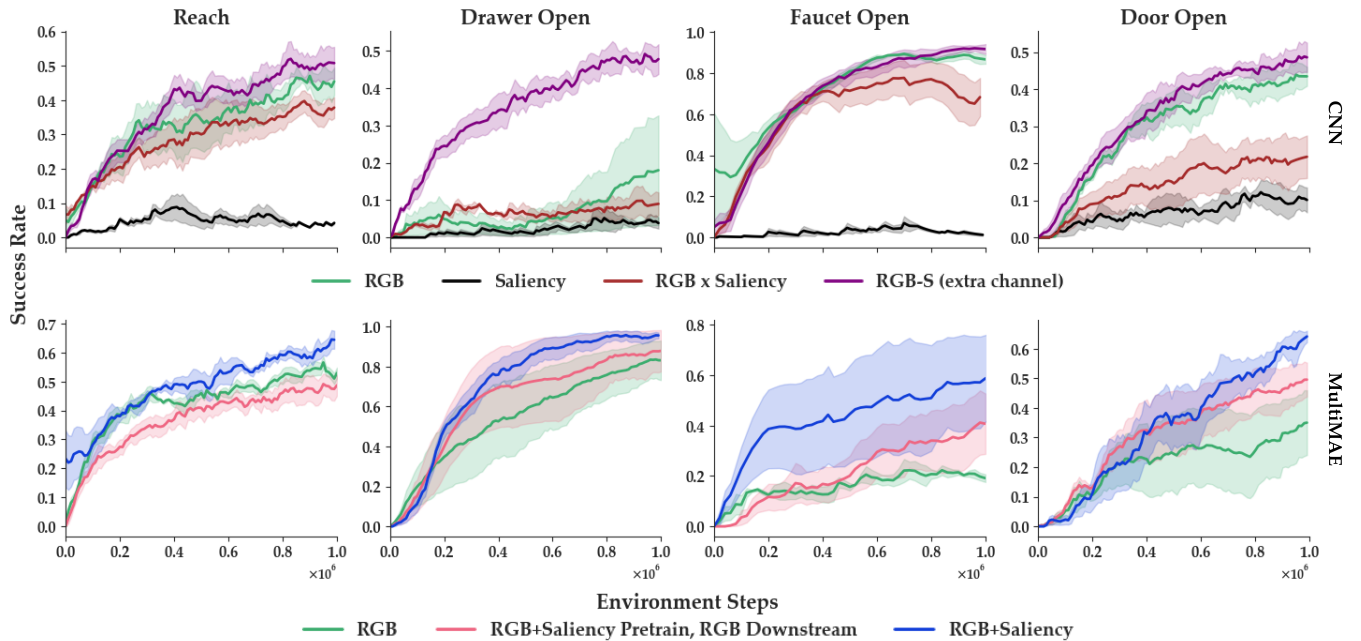


Fig. 4. **Learning curves** for four robot manipulation tasks in Meta-World evaluated by task success rate. **(Top)** CNN encoder methods. **(Bottom)** Transformer encoder methods. We select tasks that require manipulating small objects with different motions such as a pushing, pulling, and reaching. The solid lines represent the mean and shaded region the standard error across three seeds.

to a CLS token in ViT, which yielded similar results. The full procedure for ViSaRL is summarized in Algorithm 1.

#### IV. EXPERIMENT SETUP

To demonstrate the effectiveness of using human-annotated saliency information to enhance visual representations for task learning, we show quantitative results of our approach with two different encoder backbones, CNN and Transformer, across multiple simulated environments including the Meta-World manipulation [6] and DMC benchmarks [21] and real-robot manipulation with a Kinova Jaco 2 arm. We train the downstream policy using SAC [32] for the simulation experiments and behavioral cloning with expert demonstrations for the real robot experiments.

**Saliency Map Annotation.** We created a simple web-based user interface to collect saliency annotations shown in Figure 2. An annotator clicks on the pixels in the image that they think are relevant for performing the given downstream task. The interface creates a Gaussian centered around the clicked pixel with  $\sigma = 10$  on an input image of resolution  $256 \times 256 \times 3$ . For manipulation tasks, the salient regions could include the robot end-effector position, task specific objects, and the goal location.

**Quality of Saliency Prediction Model.** We find that zero-shot evaluation using a pretrained PiCANet and even state-of-the-art Vision Language Models fail to correctly identify the task-relevant regions of the image necessitating the use of human-annotation to guide the saliency training. Thus, we train a new saliency model for each task. However, we emphasize that we can learn a saliency predictor that generalizes reasonably to unseen environment states with

just five annotated examples (Figure 5). We leave training a multi-task saliency predictor for future work.

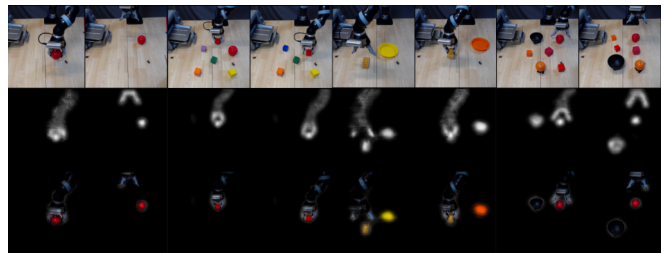


Fig. 5. **Saliency predictions** on unseen environment states. The first row is the raw RGB observations. The second row is the predicted saliency and the last row is the RGB image masked with the predicted saliency.

We apply random vertical and horizontal flip for data augmentation to prevent overfitting on our small dataset. We measure the quality of the saliency model on two evaluation metrics following prior work [29]: F-measure score ( $F_\zeta$ ) and Mean Absolute Error (MAE).

$$F_\zeta = \frac{(1 + \zeta^2) \text{Precision} \times \text{Recall}}{\zeta^2 \text{Precision} + \text{Recall}}, \quad (1)$$

where  $\zeta^2$  is set to 0.3 [29]. Saliency maps are binarized before computing  $F_\zeta$ . MAE computes the average absolute per-pixel difference between the predicted saliency maps and ground truth saliency maps. On our test dataset, we obtain an  $F_\zeta$  score of  $0.78 \pm 0.02$  and MAE of  $0.004 \pm 0.003$  averaged across all tasks, consistent with results reported in prior work [29]. Qualitative examples of the predicted saliency maps for the real-robot experiments are shown in Figure 5; further



Meta-World	CNN				MMAE		
	RGB	Saliency	RGB $\times$ Saliency	RGB(S)	RGB	RGB+Saliency (PO)	RGB+Saliency (Ours)
Reach	0.40 $\pm$ 0.12	0.04 $\pm$ 0.02	0.38 $\pm$ 0.05	0.52 $\pm$ 0.08	0.50 $\pm$ 0.02	0.48 $\pm$ 0.06	<b>0.62<math>\pm</math>0.06</b>
Drawer Open	0.18 $\pm$ 0.25	0.04 $\pm$ 0.02	0.10 $\pm$ 0.04	0.48 $\pm$ 0.06	0.84 $\pm$ 0.02	0.88 $\pm$ 0.04	<b>0.94<math>\pm</math>0.04</b>
Faucet Open	0.82 $\pm$ 0.02	0.02 $\pm$ 0.02	0.72 $\pm$ 0.16	<b>0.86<math>\pm</math>0.02</b>	0.18 $\pm$ 0.05	0.40 $\pm$ 0.20	0.62 $\pm$ 0.16
Door Open	0.42 $\pm$ 0.04	0.10 $\pm$ 0.06	0.22 $\pm$ 0.10	0.48 $\pm$ 0.06	0.36 $\pm$ 0.18	0.52 $\pm$ 0.08	<b>0.64<math>\pm</math>0.02</b>
Average	0.46 $\pm$ 0.11	0.05 $\pm$ 0.03	0.36 $\pm$ 0.08	0.58 $\pm$ 0.05	0.48 $\pm$ 0.12	0.57 $\pm$ 0.10	<b>0.65<math>\pm</math>0.07</b>

TABLE I

SUCCESS RATE ON FOUR META-WORLD MANIPULATION TASKS AVERAGED ACROSS 50 ROLLOUTS AND 3 SEEDS FOR THE CNN AND MULTIMAЕ (MMAE) VISUAL ENCODER BACKBONES. TEXT IN MAROON INDICATES THE BEST PERFORMING METHOD PER TASK.

DMControl	RGB (CNN)	CURL	RAD	RGB(S)	RGB+Saliency (PO)	RGB+Saliency (Ours)
Walker Walk	50 $\pm$ 25	895 $\pm$ 45	912 $\pm$ 38	914 $\pm$ 32	918 $\pm$ 36	<b>925<math>\pm</math>24</b>
Cartpole Swing	440 $\pm$ 43	820 $\pm$ 62	850 $\pm$ 52	838 $\pm$ 42	880 $\pm$ 37	<b>914<math>\pm</math>16</b>
Ball Catch	325 $\pm$ 55	944 $\pm$ 33	932 $\pm$ 52	939 $\pm$ 58	946 $\pm$ 62	<b>962<math>\pm</math>14</b>
Finger Spin	200 $\pm$ 180	910 $\pm$ 50	922 $\pm$ 32	933 $\pm$ 38	936 $\pm$ 16	<b>947<math>\pm</math>52</b>
Average	254 $\pm$ 76	892 $\pm$ 48	904 $\pm$ 44	906 $\pm$ 42	920 $\pm$ 38	<b>937<math>\pm</math>26</b>

TABLE II

AVERAGE EVALUATION RETURN ON FOUR DMC BENCHMARK TASKS. AVERAGE OVER 5 SEEDS EACH.

analysis can be found on the project page.<sup>1</sup>

## V. SIMULATION EXPERIMENTS

Figure 4, Table I and II summarize our main findings on four Meta-World robot manipulation tasks and five DMC tasks (Figure 6) using CNN and Transformer encoder backbones. The downstream policy is trained using Soft-Actor Critic (SAC). We additionally compare against two state-of-the-art methods for visual representation learning: CURL [3], a contrastive representation learning method and RAD [24], a method that combines various image augmentations such as color jitter and random crop to induce visual invariances in the learned representation.

**Saliency input improves downstream task success rates.** Incorporating saliency improves the task success rate in Meta-World using CNN and Transformer encoders by 13% and 18% respectively over the next best baseline. For DMC environments, we observe a 256% relative improvement in average return when using saliency input versus without. Our Transformer encoder results in an average 4% relative improvement in environment returns across all tasks over the next best prior work with a 7.5% improvement in the Cartpole Swing task.

### A. CNN Encoder

We follow the CNN implementation used in prior work [24], [21] and compare several methods for incorporating saliency. In each approach, the CNN encoder and policy are trained jointly but take different inputs.

**A saliency channel achieves the best task success rate for CNN encoder.** In Table I, we find that naive ways of utilizing saliency, such as using saliency directly as input the policy (**Saliency**), are unable to achieve good performance

on the task. We hypothesize that the saliency map alone is not sufficient to infer the exact orientation of the end-effector position critical for fine control. Supporting this hypothesis, we find that using saliency to mask the RGB observation (**RGB  $\times$  Saliency**) achieves higher task success rate than **Saliency**, but is still worse than providing the raw RGB input (**RGB**). Although masking should help the encoder identify the important image features, it may still be nontrivial for the encoder to differentiate between similarly masked observations. Lastly, we find that incorporating saliency as an additional channel to the RGB input (**RGB(S)**) improves task success rate by more than 10% across all tasks. We hypothesize that the CNN encoder is able to utilize the saliency information to more effectively associate the observed rewards to the relevant features in the image.

### B. MultiMAE Transformer

For MultiMAE experiments, the encoder is pretrained using an offline dataset of (image, saliency map) pairs. We use a 4-layer ViT encoder and a 3-layer ViT decoder with a patch size of  $8 \times 8$  pixels. We pretrain the model for 400 epochs on images collected from a random policy. The encoder weights are frozen during downstream reinforcement learning, decoupling the representation and policy learning. We compare MultiMAE representations pretrained with RGB only (**RGB**) and both RGB and saliency (**RGB+Saliency (PO)**, **RGB+Saliency (Ours)**). **RGB+Saliency (PO)** uses saliency only during pretraining while **RGB+Saliency (Ours)** uses saliency in both pretraining and downstream RL.

**Training encoder with saliency improves RGB-only success rates at inference time.** Even without saliency input during downstream RL, using saliency as an additional input modality during pretraining still improves downstream performance on 3 of the 4 tasks. Except for the Reach task, where performances are similar, **RGB+Saliency (PO)**

<sup>1</sup>The code implementation for reproducing the results and additional analysis can be found on the project website: <https://sites.google.com/view/visarl>.

	DMC-GB	CURL	RAD	RGB +Saliency (Ours)
color	Walker Walk	645±55	636±33	<b>823±55</b>
	Cartpole Swing	668±74	763±29	<b>870±21</b>
	Ball Catch	565±160	727±87	<b>962±14</b>
	Finger Spin	781±139	789±160	<b>823±102</b>
video	Walker Walk	572±121	595±85	<b>756±42</b>
	Cartpole Swing	418±72	434±58	<b>730±32</b>
	Ball Catch	402±169	520±44	<b>802±78</b>
	Finger Spin	612±55	588±82	<b>702±83</b>

TABLE III  
AVERAGE RETURN OF ViSaRL AND BASELINE METHODS ON THE COLOR AND VIDEO ENVIRONMENTS FROM DMC-GB.

achieves better success rate than RGB, with an average absolute gain of 10% across tasks.

**Using saliency in both pretraining and inference yields the best performance.** We compare the full ViSaRL method (RGB+Saliency (Ours)) to pretraining using only the RGB images (RGB) in Tables I and II demonstrating that multimodal pretraining with saliency information significantly outperforms single modality pretraining by at least a 10% margin across all tasks. Notably, RGB achieves only 19% success on Faucet Open, while our approach solves the task with 62% success rate. Using saliency as an input for both pretraining and downstream RL (RGB+Saliency (Ours)) improves task success rate over RGB+Saliency (PO) because there are new observations during online training that were not in the pretraining dataset and the encoder could benefit from the saliency input to generate a better state representation.

**ViSaRL representations generalize to unseen environments.** We evaluate the generalizability of our learned representations on the challenging *random colors* and *video backgrounds* benchmark from DMControl-GB [33]. In DMControl-GB, agents trained in the original environment are evaluated on their generalization to the same environment with visually perturbed backgrounds using randomized color and video overlays (see Figure 7). ViSaRL significantly outperforms the baselines across all tasks as shown in Table III, with an average 19% and 35% relative improvement respectively for the *color* and *video* settings. We observe that our learned saliency predictor is robust to the visual perturbations and thus the noisy background is filtered before generating the image embedding.

**Human-annotated saliency improves performance compared to depth and surface normals.** We conduct ablation experiments to compare saliency versus other mid-level input modalities such as depth and surface normals proposed by Sax et al. [27]. We substitute saliency with these other modalities as input to the MultiMAE. In Table IV, we observe that neither depth nor surface normal features alone improves task success over just using RGB image input. By contrast, adding saliency as an additional modality consistently improves task success suggesting that human-annotated saliency information can help learn better visual representations compared to other input modalities.

	Saliency	RGB	RGB + Depth	RGB + SN
Reach	✗	0.50±0.02	0.43±0.07	0.46±0.04
	✓	<b>0.62±0.06</b>	<b>0.58±0.04</b>	<b>0.64±0.06</b>
Drawer Open	✗	0.82±0.02	0.76±0.06	0.80±0.04
	✓	<b>0.94±0.04</b>	<b>0.90±0.04</b>	<b>0.92±0.04</b>
Faucet Open	✗	0.18±0.04	0.22±0.04	0.24±0.04
	✓	<b>0.62±0.16</b>	<b>0.54±0.06</b>	<b>0.58±0.10</b>
Door Open	✗	0.36±0.18	0.28±0.14	0.34±0.10
	✓	<b>0.64±0.02</b>	<b>0.62±0.04</b>	<b>0.58±0.04</b>

TABLE IV  
HUMAN-ANNOTATED SALIENCY VERSUS DEPTH AND SURFACE NORMALS (SN) AS INPUT MODALITIES TO MULTIMAE MODEL.

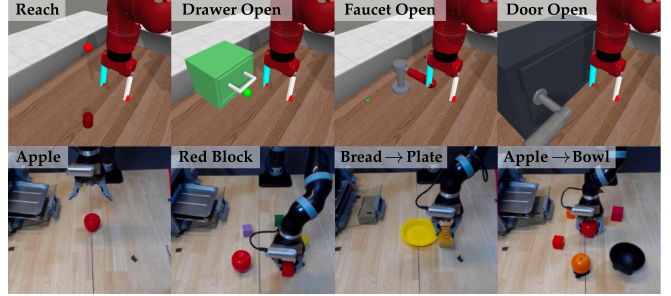


Fig. 6. **Evaluation Tasks.** Four Meta-World (top) simulation tasks and four real-robot tabletop manipulation tasks (bottom).

## VI. REAL ROBOT EXPERIMENTS

We use a Kinova Jaco 2 (6-DoF) robot arm with a 1-DoF gripper. The observation space consists of a front-view image ( $224 \times 224 \times 3$ ) from a Logitech webcam and proprioceptive information. We consider four tabletop manipulation tasks shown in Figure 6. In two of these tasks, we purposefully include distractor objects to evaluate the robustness of our learned representations to scene variations. We collected 10 demonstrations per task, resulting in an offline imitation learning dataset of around 10,000 transitions.

MultiMAE	Apple	Red Block	Bread → Plate	Apple → Bowl	Cumulative
RGB	6/10	4/10	3/10	1/10	14/40
+Saliency	8/10	7/10	6/10	6/10	27/40

TABLE V  
TASK SUCCESS RATES IN REAL-WORLD TABLETOP MANIPULATION TASKS FOR RGB AND RGB+SALIENCY WITH MULTIMAE.

For each task, 10 randomly sampled frames are hand-annotated with saliency. Even with real-world images, only a small number of annotated frames are required to learn a good saliency predictor. We train an imitation learning policy by minimizing the mean-squared error between predicted end-effector pose and expert actions. We use a recurrent policy to encode history information and a 2-layer MLP to predict continuous actions.

**ViSaRL scales to real-robot tasks and is robust to distractor objects.** Videos of evaluation trajectories for each task can be found on the project website. In Table V,

we report the task success rates on 10 evaluation rollouts. We compare MultiMAE Transformer representations trained using **RGB** and **RGB+Saliency**. Even on the easier task of `Pick Apple`, using saliency augmented representations improves the success rate. On tasks with distractor objects and longer-horizon tasks such as `Put Apple in Bowl`, saliency-augmented representations nearly double the task success rate.

## VII. CONCLUSION

We proposed to use human-annotated saliency as an additional input modality for solving challenging visual robot control tasks. We present a simple approach, ViSaRL, to utilize saliency to learn robust image representations enabling more sample-efficient and generalizable policy learning.

**Limitations and Future Work.** One potential limitation of our user interface is that it could be tedious to collect saliency annotations when scaling to more complex real world applications or video saliency [34]. Future work could investigate alternative interfaces that will enable collecting more saliency data, e.g., area-based methods or by tracking the eye gaze of the user [35].

One can further evaluate the generalizability of ViSaRL on the recent benchmark, The Colosseum [36], a suite of manipulation tasks design to measure the robustness of trained robot policies against visual perturbations.

In this paper, we only considered static frame saliency maps for single-object manipulation tasks. We plan to extend our approach to handle longer-horizon multi-object tasks using video saliency models [37] which can learn to encode more flexible temporal saliency representations across a sequence of frames. This extension could be implemented by asking the human users to watch video clips of the trajectories and annotate saliency over these clips. Another interesting direction is to investigate augmenting large-scale vision datasets with saliency to see whether saliency can benefit visual representations more generally.

## APPENDIX

**Saliency predictor training details.** Since we use a small dataset for training the saliency predictor, we apply data augmentation to prevent overfitting and improve robustness of the model. We apply VerticalFlip, HorizontalFlip and ColorJitter(brightness=0.4, contrast=0.4, saturation=0.4, hue=0.2). We use AdamW [38] optimizer with learning rate of 3e-4 and cosine learning rate annealing.

**Implementation details.** Table VI summarize the hyperparameters in ViSaRL and other baselines. ViSaRL is agnostic to the choice of downstream RL algorithm. For the CNN encoder experiments, we follow the implementation from [24], [21] and train both the encoder and policy end-to-end using Soft-Actor Critic. The encoder consist of a stack of 11 convolutional layers, each with 32 filters of  $3 \times 3$  kernels, no padding, stride of 2 for the first and 1 for all others. This results in a feature map of dimension  $32 \times 12 \times 12$  from an input image of shape  $64 \times 64 \times 3$ .

The policy head  $\pi_\theta$  and action-value functions  $Q_{\phi_i}$  are parameterized by multi-layer perceptrons. The policy head is composed of a linear projection of dimension 100 with normalization followed by 3 linear layers with 1024 hidden units each and a final linear output layer for the action prediction. As the action spaces of DMControl suite and Meta-World are continuous, the policy outputs the mean and variance of a Gaussian distribution over actions.

Hyperparameter	Value
Action repeat	1
Discount factor $\gamma$	0.99
Episode length	500
Replay buffer size	1M
Policy learning rate	Adam(lr=1e-4, $\beta_1 = 0.9, \beta_2 = 0.999$ )
$\alpha$ learning rate	Adam(lr=3e-4, $\beta_1 = 0.5, \beta_2 = 0.999$ )
Batch size	128
Target network update	2
Target network momentum $\tau$	0.05
Environment steps	1M

TABLE VI  
HYPERPARAMETERS USED IN SAC TRAINING.

**Meta-World:** The observation space is a  $64 \times 64 \times 3$  image. The action space  $\mathcal{A} \subset \mathbb{R}^4$ , is the  $\Delta(xyz)$  of the end-effector, and a continuous scalar value for gripper torque. Object and goal positions are randomized at the start of every episode to prevent exploiting spurious correlation

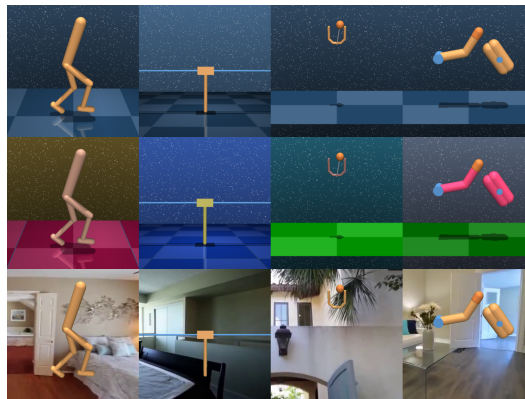


Fig. 7. **DMControl Generalization Benchmark** (Top) Four continuous control tasks from the DMControl suite. (Middle and Bottom) We evaluate on the `color.easy` and `video.easy` settings to test the generalizability of the learned representations.

**Real Robot Imitation Learning.** The downstream policy is trained using standard imitation learning. We train the saliency predictor and Transformer encoder using the same procedure outlined for the simulation experiments. Given our pretrained visual encoder, we form the state representation as a concatenation of the visual embedding and the robot proprioceptive information (e.g. joint positions). This yields a 271-dimensional state representation.

The policy is implemented as an LSTM with 256-dimensional hidden states which autoregressively predicts the actions for the next  $H$  timesteps where  $H$  is a fixed window. The state is processed by a 2-layer input MLP



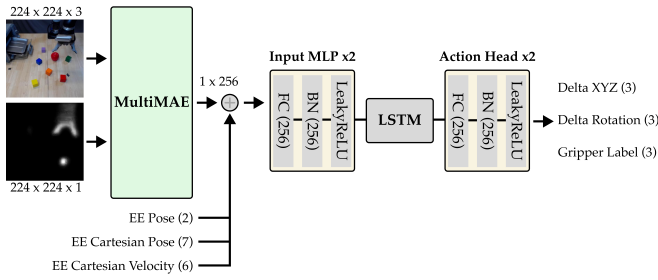


Fig. 8. **Robot Policy Architecture** We use an LSTM policy with MLPs to embed the input and generate continuous actions. The input is the cropped RGB image from an external camera and the predicted saliency map. The visual input is concatenated with the proprioceptive information.

with hidden sizes [256, 256]. The final hidden state of the LSTM is processed by a 2-layer MLP to predict a continuous action. The full model architecture is shown in Figure 8. The action space,  $\mathcal{A} \in \mathbb{R}^7$ , consists of  $\Delta(x, y, z, \phi, \theta, \psi)$ , and a continuous scalar value for gripper speed.

## REFERENCES

- [1] K. P. Darby, S. W. Deng, D. B. Walther, and V. M. Sloutsky, “The development of attention to objects and scenes: From object-biased to unbiased,” *Child development*, 2021.
- [2] L. Itti, C. Koch, and E. Niebur, “A model of saliency-based visual attention for rapid scene analysis,” *IEEE Transactions on Pattern Analysis and Machine Intelligence*, 1998.
- [3] M. Laskin, A. Srinivas, and P. Abbeel, “CURL: Contrastive Unsupervised Representations for Reinforcement Learning,” in *International Conference on Machine Learning (ICML)*, 2020.
- [4] I. Kostrikov, D. Yarats, and R. Fergus, “Image Augmentation Is All You Need: Regularizing Deep Reinforcement Learning from Pixels,” *International Conference on Learning Representations (ICLR)*, 2021.
- [5] S. Tunyasuvunakool, A. Muldal, Y. Doron, S. Liu, S. Bohez, J. Merel, T. Erez, T. Lillicrap, N. Heess, and Y. Tassa, “dm\_control: Software and Tasks for Continuous Control,” *Software Impacts*, 2020.
- [6] T. Yu, D. Quillen, Z. He, R. Julian, K. Hausman, C. Finn, and S. Levine, “Meta-World: A Benchmark and Evaluation for Multi-Task and Meta Reinforcement Learning,” in *Conference on Robot Learning (CoRL)*, 2020.
- [7] S. Cabi, S. G. Colmenarejo, A. Novikov, K. Konyushkova, S. Reed, R. Jeong, K. Zolna, Y. Aytar, D. Budden, M. Vecerik, *et al.*, “Scaling data-driven robotics with reward sketching and batch reinforcement learning,” *Robotics: Science and Systems (RSS)*, 2020.
- [8] A. Bobu, M. Wiggert, C. Tomlin, and A. D. Dragan, “Feature Expansive Reward Learning: Rethinking Human Input,” in *Human-Robot Interaction (HRI)*, 2021.
- [9] N. Wilde, E. Biyik, D. Sadigh, and S. L. Smith, “Learning Reward Functions from Scale Feedback,” in *Conference on Robot Learning (CoRL)*, 2022.
- [10] S. Tao, X. Li, T. Mu, Z. Huang, Y. Qin, and H. Su, “Abstract-to-Executable Trajectory Translation for One-Shot Task Generalization,” in *Neural Information Processing Systems (NeurIPS) Deep Reinforcement Learning Workshop*, 2022.
- [11] Y. Tong, H. Konik, F. Cheikh, and A. Tremeau, “Full Reference Image Quality Assessment Based on Saliency Map Analysis,” *Journal of Imaging Science and Technology*, 2010.
- [12] X. Wang, L. Gao, J. Song, and H. Shen, “Beyond Frame-level CNN: Saliency-Aware 3-D CNN With LSTM for Video Action Recognition,” *IEEE Signal Processing Letters*, 2016.
- [13] A. Das, H. Agrawal, L. Zitnick, D. Parikh, and D. Batra, “Human Attention in Visual Question Answering: Do Humans and Deep Networks Look at the Same Regions?” *Computer Vision and Image Understanding*, 2017.
- [14] Q. Li, Y. Zhou, and J. Yang, “Saliency Based Image Segmentation,” in *International Conference on Information and Multimedia Technology (ICIMT)*, 2011.
- [15] K. Simonyan, A. Vedaldi, and A. Zisserman, “Deep Inside Convolutional Networks: Visualising Image Classification Models and Saliency Maps,” *arXiv preprint arXiv:1312.6034*, 2013.
- [16] T. N. Mundhenk, B. Y. Chen, and G. Friedland, “Efficient Saliency Maps for Explainable AI,” *arXiv preprint arXiv:1911.11293*, 2019.
- [17] R. Zhao, W. Oyang, and X. Wang, “Person Re-Identification by Saliency Learning,” *IEEE Transactions on Pattern Analysis and Machine Intelligence*, 2016.
- [18] A. Atrey, K. Clary, and D. Jensen, “Exploratory Not Explanatory: Counterfactual Analysis of Saliency Maps for Deep Reinforcement Learning,” *International Conference on Learning Representations (ICLR)*, 2020.
- [19] M. Rosynski, F. Kirchner, and M. Valdenegro-Toro, “Are Gradient-based Saliency Maps Useful in Deep Reinforcement Learning?” *arXiv preprint arXiv:2012.01281*, 2020.
- [20] A. Boyd, P. Tinsley, K. W. Bowyer, and A. Czajka, “CYBORG: Blending Human Saliency Into the Loss Improves Deep Learning,” in *Winter Conference on Applications of Computer Vision (WACV)*, 2023.
- [21] D. Bertoin, A. Zouitine, M. Zouitine, and E. Rachelson, “Look where you look! Saliency-guided Q-networks for generalization in visual Reinforcement Learning,” *Neural Information Processing Systems (NeurIPS)*, 2022.
- [22] R. Achanta, A. Shaji, K. Smith, A. Lucchi, P. Fua, and S. Süsstrunk, “SLIC Superpixels Compared to State-of-the-Art Superpixel Methods,” *IEEE Transactions on Pattern Analysis and Machine Intelligence*, 2012.
- [23] A. Boyd, K. W. Bowyer, and A. Czajka, “Human-Aided Saliency Maps Improve Generalization of Deep Learning,” in *Winter Conference on Applications of Computer Vision (WACV)*, 2022.
- [24] M. Laskin, K. Lee, A. Stooke, L. Pinto, P. Abbeel, and A. Srinivas, “Reinforcement Learning with Augmented Data,” *Neural Information Processing Systems (NeurIPS)*, 2020.
- [25] S. Nair, A. Rajeswaran, V. Kumar, C. Finn, and A. Gupta, “R3M: A Universal Visual Representation for Robot Manipulation,” *Conference on Robot Learning (CoRL)*, 2022.
- [26] S. Karamcheti, S. Nair, A. S. Chen, T. Kollar, C. Finn, D. Sadigh, and P. Liang, “Language-Driven Representation Learning for Robotics,” *arXiv preprint arXiv:2302.12766*, 2023.
- [27] A. Sax, B. Emi, A. R. Zamir, L. Guibas, S. Savarese, and J. Malik, “Mid-Level Visual Representations Improve Generalization and Sample Efficiency for Learning Visuomotor Policies,” *Conference on Robot Learning (CoRL)*, 2019.
- [28] R. Bachmann, D. Mizrahi, A. Atanov, and A. Zamir, “MultiMAE: Multi-modal Multi-task Masked Autoencoders,” *European Conference on Computer Vision (ECCV)*, 2022.
- [29] N. Liu, J. Han, and M.-H. Yang, “PiCANet: Learning Pixel-wise Contextual Attention for Saliency Detection,” in *Computer Vision and Pattern Recognition (CVPR)*, 2018.
- [30] K. He, X. Chen, S. Xie, Y. Li, P. Dollár, and R. Girshick, “Masked Autoencoders Are Scalable Vision Learners,” in *Computer Vision and Pattern Recognition (CVPR)*, 2022.
- [31] A. Dosovitskiy, L. Beyer, A. Kolesnikov, D. Weissenborn, X. Zhai, T. Unterthiner, M. Dehghani, M. Minderer, G. Heigold, S. Gelly, *et al.*, “An Image is Worth 16x16 Words: Transformers for Image Recognition at Scale,” *International Conference on Learning Representations (ICLR)*, 2021.
- [32] T. Haarnoja, A. Zhou, K. Hartikainen, G. Tucker, S. Ha, J. Tan, V. Kumar, H. Zhu, A. Gupta, P. Abbeel, *et al.*, “Soft Actor-Critic Algorithms and Applications,” *International Conference on Machine Learning (ICML)*, 2018.
- [33] N. Hansen and X. Wang, “Generalization in reinforcement learning by soft data augmentation,” in *2021 IEEE International Conference on Robotics and Automation (ICRA)*. IEEE, 2021, pp. 13 611–13 617.
- [34] W. Wang, J. Shen, F. Guo, M.-M. Cheng, and A. Borji, “Revisiting Video Saliency: A Large-scale Benchmark and a New Model,” in *Computer Vision and Pattern Recognition (CVPR)*, 2018.
- [35] D. P. Papadopoulos, A. D. Clarke, F. Keller, and V. Ferrari, “Training Object Class Detectors from Eye Tracking Data,” in *European Conference on Computer Vision (ECCV)*, 2014.
- [36] W. Pumacay, I. Singh, J. Duan, R. Krishna, J. Thomason, and D. Fox, “The colosseum: A benchmark for evaluating generalization for robotic manipulation,” *arXiv preprint arXiv:2402.08191*, 2024.
- [37] D. Rudoy, D. B. Goldman, E. Shechtman, and L. Zelnik-Manor, “Learning video saliency from human gaze using candidate selection,” in *Computer Vision and Pattern Recognition (CVPR)*, 2013.
- [38] I. Loshchilov and F. Hutter, “Decoupled weight decay regularization,” *arXiv preprint arXiv:1711.05101*, 2017.